Available online at www.sciencedirect.com

ScienceDirect

Procedia Engineering 63 (2013) 361 – 369

Procedia Engineering

www.elsevier.com/locate/procedia

The Manufacturing Engineering Society International Conference, MESIC 2013

Study of the pore formation on CoCrMo alloys by selective laser melting manufacturing process

K. Monroy[a], J. Delgado[a], J. Ciurana[a,]*

[a]*Department of Mechanical Engineering and Civil Construction, Universitat de Girona, Av. Lluis Santaló s/n, 17071, Girona, Spain.*

Abstract

Cobalt-base alloys are widely used in medical applications as is the hardest known biocompatible alloy along with a high wear and/or corrosion resistance. The manufacturing process used on these alloys strongly influences the features produced, therefore it should be carefully controlled to attain the desired quality. Selective laser melting (SLM) is a novel process proposed for the fabrication of biomedical implants with cobalt alloys. In this technique, density is the most important concern as it has a direct influence on the component performance. Due to its different energy inputs given by its processing parameters, it has the potential to control porosity through them. In this work, SLM experiments were carried out on a CoCrMo alloy to study the formation of pores. The analysis showed that the SLM technique enables the building of high dense samples up to 99%, resulting in a mean of porosity of 5.77% and a pore mean size of 0.759 μm^2.

Keywords: selective laser melting; additive manufacturing; cobalt alloys; porosity.

1. Introduction

Over the years cobalt-chromium-molybdenum (CoCrMo) has demonstrated a remarkable level of versatility and durability as an orthopaedic implant material. These alloys are widely used in biomedical applications as is the hardest known biocompatible alloy along with good tensile and fatigue properties. Originally they were adopted for dental applications and lately they have been employed for body joints and fracture fixation applications. How these alloys are manufactured can markedly affect the mechanical and metallurgical properties of the resulting

* Corresponding author. Tel.: +34 972 418 829; fax: +34 972 418 098. *E-mail address:* quim.ciurana@udg.edu

doi:10.1016/j.proeng.2013.08.227

components, therefore it should be carefully controlled to attain the desired quality. Investment casting and closed die forging remain the traditional processes used to manufacture cobalt-chromium-molybdenum alloy implants. Nevertheless, additive manufacturing (AM) is being proposed as the novel candidate for the fabrication of customized biomedical implants with the cobalt alloys (Ram et al., 2008; Berlin et al., 1999).

Additive Manufacturing (AM) is one of the most developed technologies in recent years, it includes techniques as stereolithography (SLA), Selective Laser Sintering (SLS), Layer Object Manufacturing (LOM), Fused Deposition Modeling (FDM), 3-Dimentional Printing (3DP, and Selective Laser Melting (SLM) (Delgado et al., 2011). Among them, SLM is now being highly demanded since it offers a lower time-to-market, a near-net-shape production, a higher material utilization rate, along with its ability to produce functional metallic parts with mechanical properties comparable to those in bulk materials (Kruth et al., 2005 and Gu et al., 2012).

The SLM technology consists of building three dimensional objects layer by layer through melting selectively a metal powder using laser radiation. SLM, compared to the classical laser sintering, requires higher energy levels, which are normally achieved by applying a high laser power and by using thin powder layer thickness. Therefore, it suffers from several issues associated with the melting and consolidation phenomena of the metallic powders (Gu et al., 2012). Typical concerns from the melt instability and large thermal stresses generated in the material include balling effect, porosity, lack of fusion, part distortion, cracks and delaminations. Among these defects, porosity is the most frequently reported in many metallic pieces manufactured by SLM. Moreover, it is the most important concern in this process as it is well known that it is detrimental to the mechanical properties, since pores act as stress concentrators leading to an earlier onset of plasticity and localizations of strains. Both morphology and distribution of pores in the component can have a significant effect on the mechanical behavior, and in turn, on the component performance (Kruth et al., 2000, Yadroitsev et al., 2009, Dadbakhsh et al., 2012).

The ideal objective in SLM is to obtain 100% dense parts, which means zero porosity, which is a challenge in the field due to a lack of mechanical pressure, as in moulding processes. By its counterpart, SLM is only characterized by temperature effects, gravity and capillary forces. In fact, porosity in the final part still remains a challenge even for conventional production techniques (Kruth et al., 2000).

Previous studies have shown that SLM has the potential of controlling porosities according to the capacity of providing different energy inputs by its processing parameters (Li et al., 2010). In this work, SLM was applied on a CoCrMo powder to study the formation of pores and its relation with the processing conditions in order to understand its development and to control this setback.

2. Experimental Methodology

2.1. Material

Cobalt-chromium-molybdenum powder was used for the SLM experiment. The powder particles exhibited predominantly spherical morphology (Fig. 1b) with diameter sizes between 20 to 50 μm (Fig. 1a).

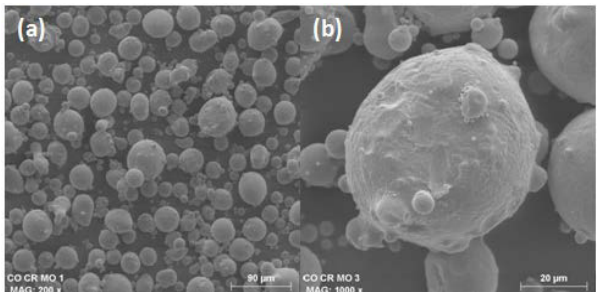

Fig. 1. SEM images showing the CoCrMo powder particle morphology (a) Mag. 200x (b) Mag. 1000x. (Delgado et al., 2011b)

The powder chemical composition, listed on Table 1, was semi-quantitatively determined by Energy-Dispersive X-ray (EDX).

Table 1. Chemical composition of the CoCrMo powder

Element	Cobalt	Chromium	Molybdenum
Content (wt. %)	60.25	31.62	8.14

2.2 *Equipment*

In this experiment, a self-develop SLM machine was used, depicted in Fig. 2. The system consisted on a vertical milling centre equipped with an Ytterbium-fiber laser type (FL x50s, Rofin) which operates at a maximum power of 500W in continues wave at a 1080 nm of wavelength. The welding head was equipped with a focal length and collimator of 125mm producing a minimum spot size of 150 μm. The powder layers were deposited on a building platform plate of Steel AISI 1045 with a built inclined plane which permitted the evaluation of the process at different layer thicknesses.

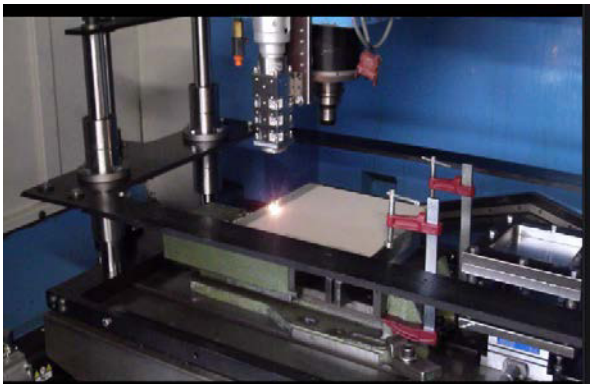

Fig. 2. Vertical milling centre equipped with an Ytterbium-fiber laser type

2.3 *Single track forming process*

To simplify the interpretation, samples were built using a straight laser scan, as shown in Fig. 3. Each experiment consisted on a single track of 230 mm in length, where the powder layer thickness was varied continuously from 40 to 500 mm. The building process was specified under four families or groups of experiments. Each family corresponded to a different scan speed value, and within each family the straight tracks were produced under different laser power values. The summary of the factorial design of experiments (DOE) used on the deposition are listed on Table 2. The SLM process was performed without a controlled atmosphere.

Table 2. Design of Experiments. Factors and levels

Runs	Parameters	Min	Max	Increment
80	P [W]	25	500	25
	SS [mm/s]	33.3	83.3	16.7
	LT [μm]	40	500	Continuous

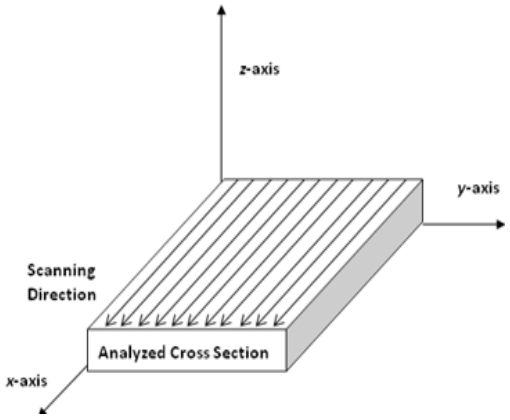

Fig. 3. Scanning strategy used on SLM experiments Based from (Kruth et al. 2005, Delgado et al., 2011b)

2.4 Porosity Characterization

The outcome of the SLM testing was a platform containing 80 samples. The samples were then prepared by standard metallographic technique; the plate was cut from a cross section view by Wire Electrical Discharge Machining (WEDM), mounted on epoxi resin RSF 816 and grounded using a SiC paper through fine 2000 grit size. After grinding, polishing was done with alumina suspension on 9.5, 3 and 1 μm synthetic cloths. In order to quantify the porosity and the pore mean size cross section images performed on Leica microscopy were used. The images where binarized using a threshold value. Then the porosity was calculated as the ratio of the black to white pixels (shown in Fig. 4), which represented the fraction of the surface voids over the total surface. The pore mean size was acquired by particle analysis in ImageJ software.

Finally, the obtained data was statistically studied by analysis of variance (ANOVA) to determine the effect of the laser power (P), scanning speed (SS) and layer thickness (LT) and its interaction, on the porosity and pores formed during the experimental study.

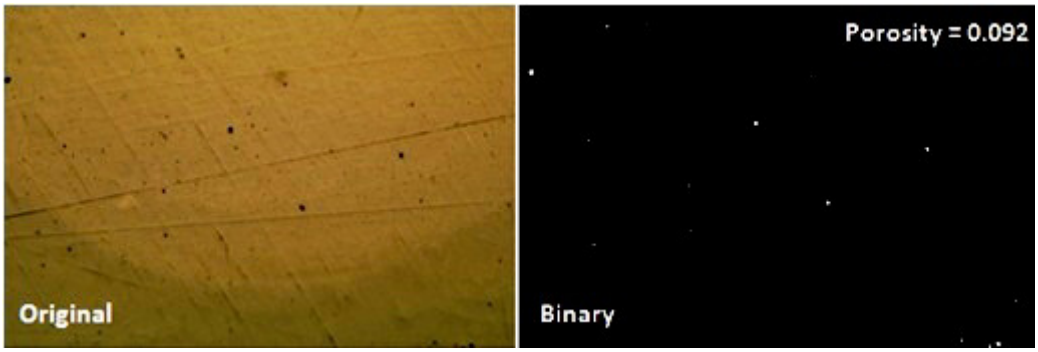

Fig. 4. Binary treated image, (SS= 50 mm/s, LT= 100 μm and P=425 W). Mag. 200x

3. Results and discussion

During the sintering, the total solid volume may be maintained and to reach this constant value, the shape and size of each particle change with the formation of grain boundaries. This change in solid particles is accompanied

by the change of shape, size and fraction of pores in a unit volume. Therefore, since the aim of this research is to describe and study the pore characteristics formed on CoCrMo during SLM, the porosity along with pore morphology features as pore shape, size, and distribution will be presented in this section given that they have a profound impact on the mechanical behavior of the component. Furthermore, the presented results were analyzed to encounter the controllable relation with some process parameters (Kruth et al., 2000, Yadroitsev et al., 2009, Dadbakhsh et al., 2012).

3.1 Porosity

Primary porosity focuses on the larger pores which are due primarily to the powder packing characteristics. The densification of these powder particles is the main purpose of the selective laser melting process. Therefore, the final primary porosity depends on the particle sizes of the initial CoCrMo powder, given that the compaction process starts with the rearrangement of these powder particles. Consequently, it can be said that using a distribution of diverse size particles (from 20 μm to 50 μm), as on the present experiment, can ensure a good interdiffusion of the components into one another through vacancy movements and by large surface contact, which subsequently permitted to overstep from an initial porosity of 39.63% (Fig. 6a) (Salak, 1997; Chawla and Deng, 2005; Angelo and Subramanian, 2008) to a lowest value of 0.9% and a 5.77% mean of porosity.

3.2 Pore Shape

Fig. 6, a micrograph of the SLM sample cross section, shows the shapes of the present pores. Two different shape types of pores are distinguishable: round pores, which are formed during the sintering process; and irregular pores, which are formed during the compacting process.

The predominant shape encountered was the round pores, where its circularity resulted from 0.79 to 0.919; numbers that reflect the regularity of the shape in the formed pores. In general, the literature states that irregular pores have a higher stress than perfectly round pores (Chawla and Deng, 2005). Moreover, irregular pores are a matter of serious concern as they evidence the faulty powder deposition and/or abrupt changes in powder environment, geometry or scanning conditions requiring a bigger effort for process optimization.

The contour of the round pores was characterized, observing to be rough and smooth walls. Pores found with smooth walls came from the final stage of densification, were pores become isolated and any gas remaining becomes trapped, the rough walls can be derived by dendrite contraction.

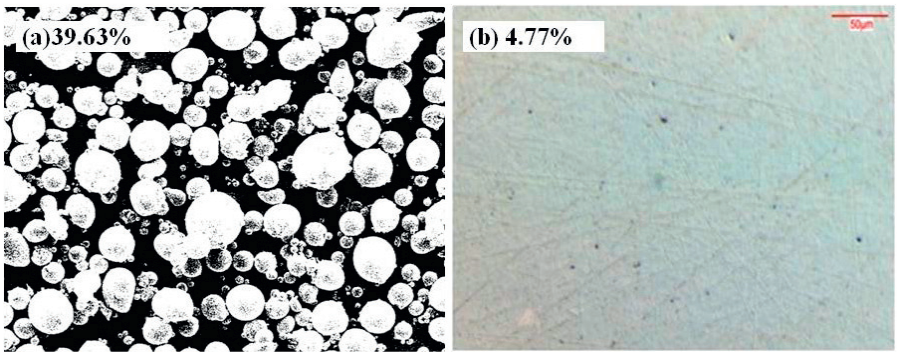

Fig. 5. (a) Initial powder and (b) after SLM sample porosity (SS= 83.33 mm/s, P= 475 W, LT= 400 μm). Mag. 200x

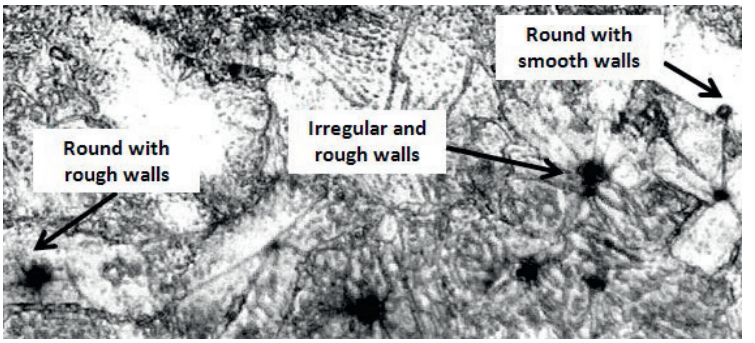

Fig. 6. Pore morphology (SS=33 mm/s, P=350-500 W, LT= 50 μm). Mag.500x

3.3 Pore Distribution

In pore distribution studies, the structures are characterized in two main categories: regular porous structures and irregular porous structures. In this experiment, the pore architecture does not exhibit an orderly geometry and the pore formation was random, therefore exhibiting irregular porous structures. In Fig. 7 is presented a section of a part produced by SLM in which it can be seen that the pore formation is arbitrary and homogeneously distributed in each cross section.

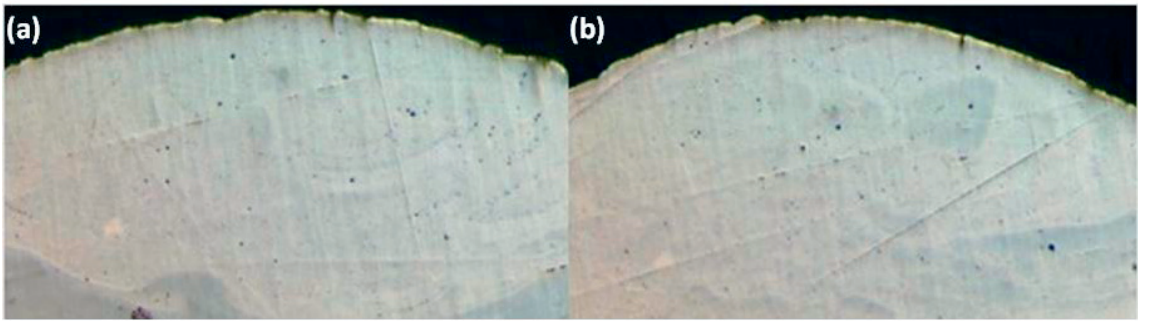

Fig. 7. Porosity allocation (LT=100 μm, SS=66) a) 425 W and b) P=450 W. Mag. 200x

3.4 Pore Size

Depending on the size, pores can be classified as micro-pores (<0.002 μm), meso-pores (0.002 – 0.05 μm) and macro-pores (>0.05 μm) (Sing, 1985). The total amount of pores developed in the experiment belongs to the category of macropores, as the mean pore diameter was 0.9454 μm and the size, 0.759 μm^2. Statistically 95% of the pores were found to have a diameter between 0.9199 and 0.9710 μm.

3.5 Influence of Processing Conditions

A statistical analysis was performed to calculate the variation and the influence of all the process parameters during the experiments. In the current study, the process parameters considered were: the laser power (P), the laser scan speed (SS), and the layer thickness (LT). Porosity and pore mean size of sintered parts were evaluated as output variables. Moreover, as the interactions between the input parameters also resulted in variations on the porosity and pore mean size, they were also quantified as influential effects of the experiment.

The general factorial DOE analysis states that the mean of all the measured porosities (%) and pore mean size (μm^2) of tested parts were 5.77 and 0.759 μm^2, respectively. The above results and the calculated effects are presented in Tables 3 and 4.

Table 3. ANOVA Table -Porosity

Source	df	SS	MS	F	p-value
LT	9	0.122	0.0135	24.54	2.42E-16
SS	3	0.004	0.0015	2.778	0.0494
P	14	0.009	0.0006	1.236	0.2762
LT*SS	27	0.100	0.0037	6.712	1.1E-09
LT*P	118	0.113	0.0009	1.747	0.0104
SS*P	42	0.033	0.0008	1.457	0.0934
LT*SS*P	159	0.167	0.0010	1.906	0.0031
Error	56	0.030	0.0005		
Total	428	0.582	0.0228		

Table 4. ANOVA Table –Pore size

Source	df	SS	MS	F	p-value
LT	9	2.994	0.332	2.133	0.0414
SS	3	9.714	3.238	20.76	3.5E-09
P	14	3.597	0.256	1.647	0.0945
LT*SS	27	21.04	0.779	4.997	1.9E-07
LT*P	118	26.53	0.224	1.441	0.0635
SS*P	42	8.614	0.205	1.315	0.1677
LT*SS*P	159	27.348	0.172	1.102	0.3423
Error	56	8.733	0.1559		
Total	428	108.57	5.3652		

As seen in the tables and in the statistical analysis, the main effects are highly significant, being LT for most influent factor for porosity and SS for pore size. Although not as high as the main effects, the interaction LT*SS, also presented evidence of substantial effect on both, porosity and pore mean size. The results showed that the porosity is reduced by increasing the layer thickness; and that is almost independent of the scanning speed. The latter trend can be seen visually on the Fig. 8. This phenomenon may be explained as with a high layer thickness, a good particle packing is more likely to occur. Consequently, a greater contact area takes place and in consequence, a more effective thermal conductivity, a fuller densification and at last, a successful pore removal or shrinkage can occur.

By the counterpart, the pore mean size remained equal under different layer thickness and laser power conditions, while at lower scanning speeds the pore mean size increased a noticeable 41.17% (Table 5). Changes like recrystallization and grain growth, during sinterization may explain this occurrence. Based in the latter, the grain growth permits the densification and the removal or shrinkage of the pores. However, if high temperatures are maintained for extensive long times during sintering, as with lower scanning speeds, the pore growth can be promoted. As it was reported by Simchi (2006), the low scan rates can also decrease the density by contributing to the formation of large cracks and delamination of the sintered layers.

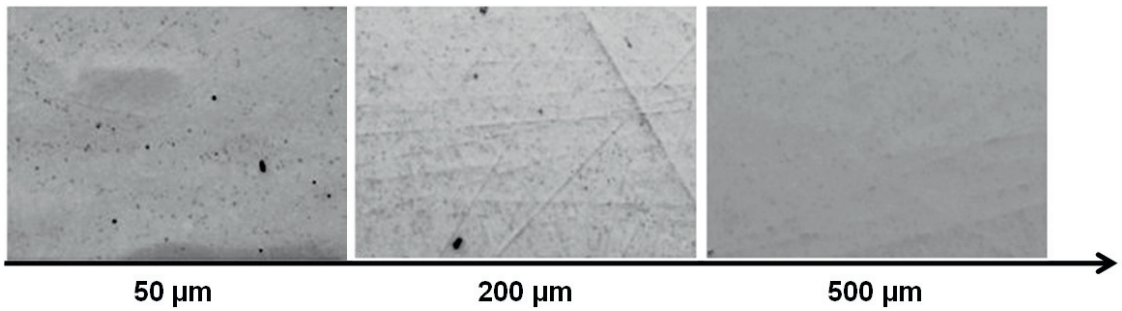

Fig. 8. Effect of layer thickness on porosity

Table 5. Pores mean size (μm^2) and pore diameter, d (μm) by Scanning Speed (SS)

SS, mm/s	Pore mean size, μm^2	Pore d, μm
33.33	0.943	1.054
50	0.690	0.904
66.6	0.646	0.887
83.33	0.633	0.881

Initial efforts of the research were concentrated on determining the processing window for optimizing porosity issues. In the case of porosity, considering only the significant factors, the minimum porosity (2.00%) was acquired with the SS level of 50-66.6 mm/s interacting with the highest layer thickness, 500 μm (shown in Fig. 9a). The smallest pores (0.197 μm2) were formed by a high level of scanning speed, 83.3 mm/s, interacting with a 500 μm layer thickness (Fig. 9b).

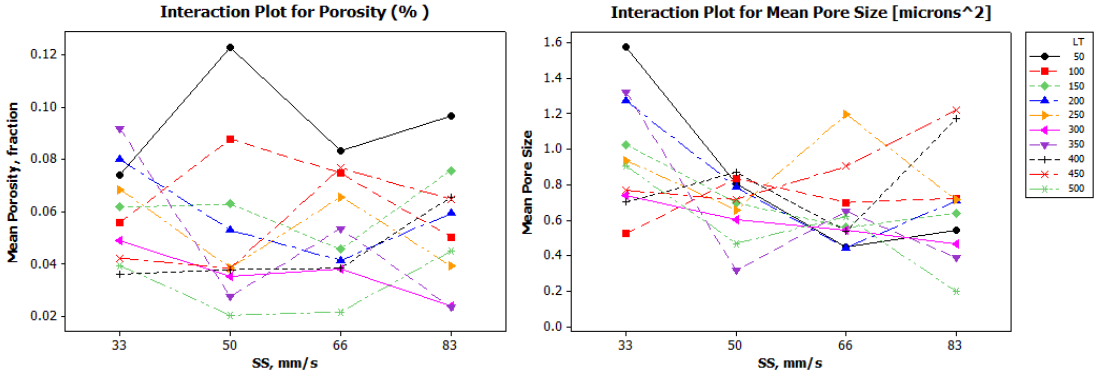

Fig. 9. Interaction plots for porosity (left) and pore mean size (right in μm^2) versus LT*SS

4. Conclusions

In this study porosity features and its relation with SLM were systematically studied. The following conclusions can be made based on the results:

- The image analysis shows mainly round pores with smooth walls which came from gas entrapment. These were found in random allocation and all over the cross section of the sample.
- The SLM technique enabled the building of high dense samples, reaching a lowest 0.9% of porosity, and a mean of 5.77%.
- The minor porosity was produced by the highest layer thickness, which provided a better particle packing enhancing then the thermal conductivity among the particles and subsequently permitting a successful densification and finally the pore removal or shrinkage.
- The pore mean size, 0.759 μm^2, remained equal under different layer thicknesses and laser power conditions; while at lower scanning speeds the pore mean size increased a noticeable 41.17%. The literature states that if high temperatures are maintained for long times during sintering, pore growth will occur. This condition is fulfilled with lower scanning speeds, by which the exposure time to the laser radiation extends and therefore pore growth occurs.

- The optimized process window stated that minimum porosity was obtained with a scanning speed level of 50 mm/s interacting with the highest layer thickness, 500 μm. The smallest pores (0.197 μm^2) were formed by a scanning speed level of 83.3 mm/s, and a 500 μm layer thickness.

Acknowledgements

The authors gratefully appreciate the financial supports from the University of Girona BR09/04, the Spanish Government (project DPI2009-09852). The research leading to these results has received funding from the European Union Seventh Framework Programme (FP7-PEOPLE-2009) under the grant agreement IRSES nº 247476.

References

Angelo, P.C., Subramanian, R., 2008. Powder Metallurgy: Science, Technology and Applications. PHI Learning Private limited, New Delhi, pp. 144.

Berlin, R.M., Gustavson, L.J., Wang, K.K., 1999. Influence of Post Processing on the Mechanical Properties of Investment Cast and Wrought Co-Cr-Mo Alloys. In: Disegi, J.A., Kennedy, R.L., Pilliar, R (Eds.), Cobalt-Base Alloys for Biomedical Applications. ASTM STP 1365, American Society for Testing and Materials, West Conshohocken, PA, pp. 62-70.

Chawla, N., Deng, X., 2005. Microstructure and mechanical behavior of porous sintered steels. Materials Science and Engineering A 390, 98–112.

Dadbakhsh, S., Hao, L., Sewell, N., 2012. Effect of selective laser melting layout on the quality of stainless steel parts. Rapid Prototyping Journal 18, 241–249.

Delgado, J., Serenó, L., Ciurana, J., Hernández, L., 2011a. Influence of process parameters in the first melting layer of a building platform in a SLM machine. In: Bartolo, P.J. et al. (Eds.). Innovative Developments in Virtual and Physical Prototyping, CRC Press, London, UK, pp. 499–502.

Delgado, J., Serenó, L., Ciurana, J., Hernández, L., 2011b. Methodology for analyzing the depth of sintering in the building platform. In: Bartolo, P.J. et al. (Eds.). Innovative Developments in Virtual and Physical Prototyping, CRC Press, London, UK, pp. 495-498.

Gu, D., Hagedorn, Y.C. Meiners, W., Meng, G., Santos Batista, R.J., Wissenbach, K., Poprawe, R., 2012. Densification behavior, microstructure evolution, and wear performance of selective laser melting processed commercially pure titanium. Acta Materialia 60, 3849-3860.

Janaki R., G.D., Esplin, C.K., Stucke, B.E., 2008. Microstructure and wear properties of LENS deposited medical grade CoCrMo. Journal of Materials Science: Materials in Medicine 19, 2105-2111.

Kruth, J.P., Badrossamay, M., Yasa, E., Deckers, J., Thijs, L., Van Humbeeck, J., 2000. Part and material properties in selective laser melting of metals. In: Wan Sheng, Z., Jun, Y (Eds.). Proceedings of the 16th International Symposium on Electromachining, Shanghai Jiao Tong University Press, Shangai, China.

Kruth, J.P., Mercelis, P., Van Vaerenbergh, J., Froyer, L., Rombouts, M., 2005. Binding mechanisms in selective laser sintering and selective laser melting. Rapid Prototyping Journal 11, 26–36.

Li, R., Liu, J., Shi, Y., Du, M., Xie, Z., 2010. 316L Stainless Steel with gradient porosity fabricated by selective laser melting. Journal of Material Engineering and Performance 19, 666-671.

Salak, A, 1997. Ferrous Powder Metallurgy, Cambridge International Science Publishing, Cambridge, pp. 38-60.

Simchi, A., 2006. Direct laser sintering of metal powders: Mechanism, kinetics and microstructural features. Materials Science and Engineering A 428, 148–158.

Sing, K.S.W., 1985. Reporting physisorption data for gas/solid systems with special reference to the determination of surface area and porosity. Pure and Applied Chemistry 57, 603-619

Yadroitsev, I., Pavlov, M., Bertand P.H, Smurov, I., 2009. Mechanical properties of samples fabricated by selective laser melting. In: 14th European Meeting Prototyping & Rapid Manufacturing, Paris, France.